

# Systematic Features and Progenitor Dependence of Core-collapse Supernovae

KO NAKAMURA<sup>1,2</sup>, TOMOYA TAKIWAKI<sup>3</sup>, TAKAMI KURODA<sup>4</sup>, and KEI KOTAKE<sup>5,3</sup>

<sup>1</sup>*Yukawa Institute for Theoretical Physics, Kyoto University, Kitashirakawa Oiwakecho, Sakyo-ku, Kyoto 606-8502, Japan*

<sup>2</sup>*Faculty of Science and Engineering, Waseda University, 3-4-1 Ohkubo, Shinjuku-ku, Tokyo 169-8555, Japan*

<sup>3</sup>*National Astronomical Observatory of Japan, 2-21-1 Osawa, Mitaka, Tokyo 181-8588, Japan*

<sup>4</sup>*Department of Physics, University of Basel, Klingelbergstrasse 82, 4056 Basel, Switzerland*

<sup>5</sup>*Department of Applied Physics, Fukuoka University, 8-19-1 Nanakuma Jonan, Fukuoka 814-0180, Japan*

*E-mail: nakamura.ko@heap.phys.waseda.ac.jp*

(Received August 21, 2016)

We present our latest results of two-dimensional core-collapse supernova simulations for about 400 progenitors. Our self-consistent supernova models reveal the systematic features of core-collapse supernova properties such as neutrino luminosity and energy spectrum, explosion energy, remnant mass, and yield of radioactive <sup>56</sup>Ni. We find that these explosion characteristics tend to show a monotonic increase as a function of mass accretion rate onto a shock. The accretion rate depends on the structure of the progenitor core and its envelope, which is well described by the compactness parameter.

**KEYWORDS:** Hydrodynamics, Neutrinos, Nucleosynthesis, Supernovae

## 1. Introduction

The explodability of massive stars and their explosion properties depend sensitively on the pre-supernova structures. In this article, we present our neutrino-radiation hydrodynamics simulations in two dimensions using the whole pre-supernova series (101 solar-metallicity models, 247 ultra metal-poor models, and 30 zero-metal models) of Woosley et al. (2002) [1]. We can self-consistently follow a supernova evolution starting from the onset of core-collapse, bounce, neutrino-driven shock-revival, until the revived shock comes out of the iron core. The goal of our 2D models is to study the systematic dependence of the shock revival time, diagnostic explosion energy, mass of remnant object, and nucleosynthetic yields on the progenitors' structure.

## 2. Numerical Scheme

Our 2D models are computed on a spherical polar grid of 384 non-equidistant radial zones from the center up to 5000 km and 128 equidistant angular zones covering  $0 \leq \theta \leq \pi$ . To solve spectral transport of electron and anti-electron neutrinos, we employ the isotropic diffusion source approximation (IDSA) with a ray-by-ray approach. We take into account explosive nucleosynthesis and the energy feedback into hydrodynamics by solving a 13  $\alpha$ -nuclei network including <sup>4</sup>He, <sup>12</sup>C, <sup>16</sup>O, <sup>20</sup>Ne, <sup>24</sup>Mg, <sup>28</sup>Si, <sup>32</sup>S, <sup>36</sup>Ar, <sup>40</sup>Ca, <sup>44</sup>Ti, <sup>48</sup>Cr, <sup>52</sup>Fe, and <sup>56</sup>Ni. The nuclear energy compensates for energy loss via endothermic decomposition of iron-like NSE nuclei to lighter elements [2]. See Nakamura et al. (2015) for more details [3].

### 3. Results

For all the computed 378 models, the bounce shock stalls in a spherically symmetric manner and only after that, we observe a clear diversity of the multi-D hydrodynamics evolution in the postbounce phase. Figure 1 shows a snapshot of entropy distribution for selected 48 solar-metallicity models at 400 ms after bounce. These models have a variety of shapes and radii of their shock fronts. At this time, the shock of the most massive progenitor (s75.0) is reaching an average radius of 1000 km, whereas the shock of s24.0 is still wobbling around at  $\sim 200$  km. This implies that the initial zero-age main-sequence (ZAMS) mass is not a good criterion to diagnose the possibility of explosion.

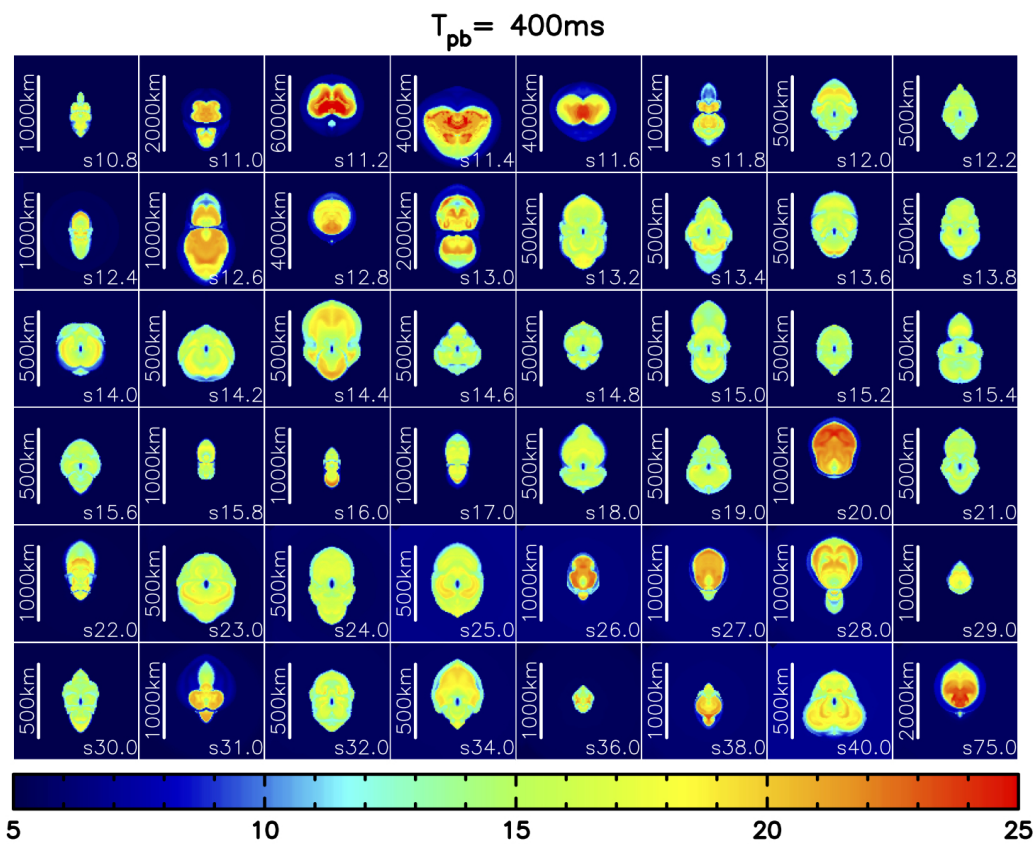


**Fig. 1.** Entropy distributions at 400 ms postbounce in unit of  $k_B$  per baryon for selected 48 models with solar metallicity. Shown are models s11.2 to s75.0, from top-left to bottom-right. Note the different scale in each panel.

The diversity is also seen in another supernova properties. Figure 2 shows time evolution of electron neutrino luminosity for 101 solar-metallicity models. The difference of the luminosity between the highest and the lowest model is more than a factor of three. The left panel of Figure 2 presents a dependence of the neutrino luminosity on the ZAMS mass of progenitors. Massive progenitors colored by red lie not on the top but in-between, which again suggest the ZAMS mass has a less ability to predict supernova properties such as the neutrino luminosity.

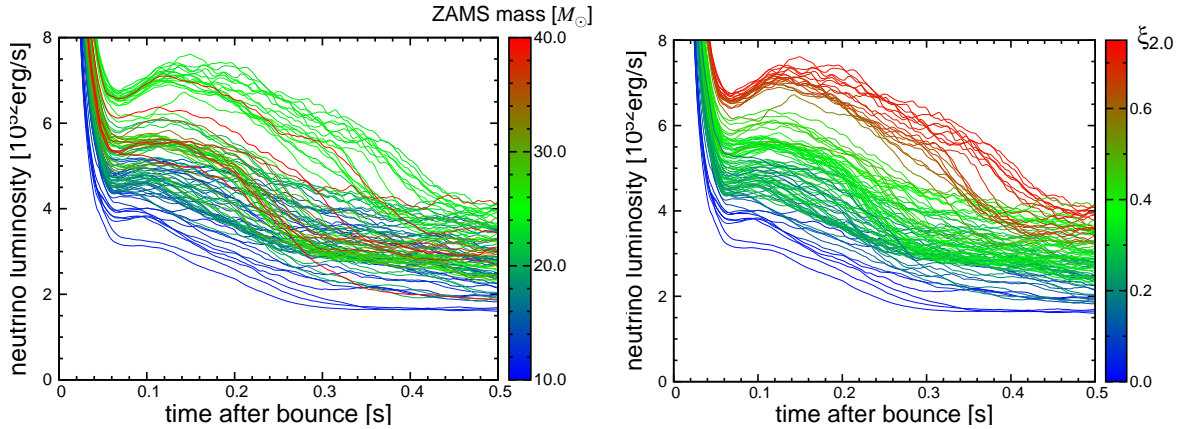


**Fig. 2.** Electron neutrino luminosity colored by ZAMS mass (left panel) and the compactness parameter  $\xi_{2.0}$  (right panel).

Here we introduce the compactness parameter [4] defined as the ratio of mass  $M$  and the enclosed radius  $R(M)$ ,

$$\xi_M = \frac{M / M_\odot}{R(M) / 1000 \text{ km}}. \quad (1)$$

This parameter characterizes a density structure of a progenitor star within the chosen mass coordinate  $M$ . Once we take the compactness, in place of the ZAMS mass, the neutrino luminosities of 101 supernova models present a clear increasing trend (right panel in Figure 2). This is because the neutrino luminosity at a few hundred ms after bounce is dominated by an accretion luminosity and the compactness parameter is tightly correlated to a mass accretion rate onto the shock. In this article, we estimate  $\xi_M$  at  $M = 2.0M_\odot$ . Different choices of  $M$ , for example  $M = 2.5M_\odot$ , do not change our conclusions, although too small  $M$  ( $\lesssim 1.5M_\odot$ ) is not suitable to characterize the shock behavior.

Metal-deficient progenitors also follow this trend. The top-left panel of Figure 3 shows the electron neutrino luminosity of all the examined 378 models as a function of the compactness parameter  $\xi_{2.0}$ . Here the neutrino luminosity is estimated at the shock revival defined as the time when the average shock radius reaches 400 km. Not only the solar metallicity models (black dots), but also ultra metal-poor models (blue) and zero-metal models (red) present a linearly increasing trend.

The gravitational mass of proto-neutron star (PNS) at the final simulation time is shown in the top-right panel of Figure 3. Here the PNS is defined by the region where the density  $\rho > 10^{11} \text{ g cm}^{-3}$ . The PNS mass is almost converged in our simulation time and the value at the final simulation time has a clear correlation with the compactness parameter. The PNS masses of the models with very high  $\xi_{2.0}$  ( $\gtrsim 0.7$ ) seem to be very large ( $\sim 2.2M_\odot$ ). Here it should be noted that the PNS soon after bounce is still hot. At this phase, the contribution of thermal pressure cannot be neglected, so that these massive PNS can resist collapsing to form black holes.

Explosion energies (bottom-left panel) and synthesized  $^{56}\text{Ni}$  masses (bottom-right panel) also present the increasing trend as a function of the compactness parameter. This can be interpreted as follows: the core of high-compactness models is surrounded by high-density Si/O layers and the mass accretion rate therefore remains high long after the stalled shock has formed. This makes the PNS

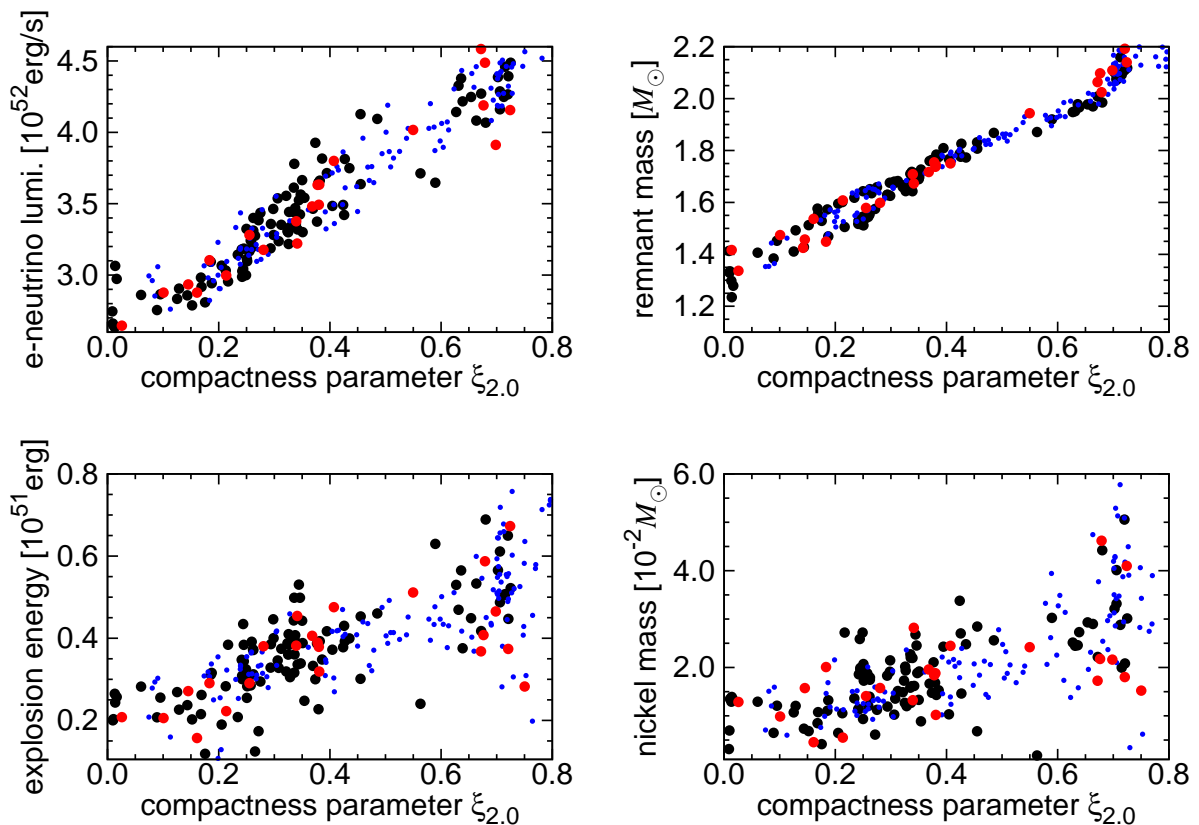


**Fig. 3.** Explosion properties as a function of the compactness parameter  $\xi_{2.0}$ . Different colors present different metallicity of progenitors (solar-metallicity models in black, ultra metal-poor models in blue, and zero-metal models in red).

mass of the high-compactness models heavier. Due to the high accretion rate, the accretion neutrino luminosities become higher for models with high compactness. As a result, we obtain a stronger shock revival powered by the more intense neutrino heating, which makes the amount of the synthesized nickel bigger.

The explosion energy for the 101 models is in the range between  $\sim 0.1 - 0.7 \times 10^{51}$  erg, which is still increasing at the final time of our simulation. To obtain a converged value of the explosion energy, we need to perform a very long-term simulation including the special care about the smooth transition of the EOS to the non-NSE regime, which will be reported in near future. This study is based on 2D simulations. Recent 3D simulations (e.x., Lentz et al. 2015 [5]) show that the onset of explosion is delayed relative to 2D models. The effects on explosion properties as well as systematic trends should be examined in more detail.

### Acknowledgements

This study was supported in part by JSPS KAKENHI Grant Number 16K17668.

### References

- [1] S. E. Woosley, A. Heger, and T. A. Weaver: *Rev. of Mod. Phys.* **74** (2002) 1015
- [2] K. Nakamura, T. Takiwaki, K. Kotake, and N. Nishimura: *ApJ* **782** (2014) 91
- [3] K. Nakamura, T. Takiwaki, T. Kuroda, and K. Kotake: *PASJ* **67** (2015) 107
- [4] E. O'Connor, and C. D. Ott: *ApJ*, **730** (2011) 70
- [5] E. J. Lentz, S. W. Bruenn, W. R. Hix, et al.: *ApJL*, **807** (2015) L31